



Study of the Effect of ACL Anode Catalytic Layer Porosity on the Efficiency of a Direct Methanol Fuel Cell

Mihoub Medkour¹, Noureddine Kaid², Houari Ameer², Chutarat Tearnbucha^{3*}, Weerawat Sudsutad⁴, Giulio Lorenzini⁵, Hijaz Ahmad^{6,7}, Younes Menni²

¹ Département des Sciences et de la Technologie, Faculté des sciences et de la Technologie, Université de Tissemsilt, Tissemsilt 38000, Algeria

² Department of Technology, University Centre of Naama (Ctr Univ Naama), P.O. Box 66, Naama 45000, Algeria

³ Department of General Education, Faculty of Science and Health Technology, Navamindradhiraj University, Bangkok 10300 Thailand

⁴ Department of Statistics, Faculty of Science, Ramkhamhaeng University, Bangkok 10240, Thailand

⁵ Department of Engineering and Architecture, University of Parma, Parco Area delle Scienze, 181/A, 43124 Parma, Italy

⁶ Information Technology Application and Research Center, Istanbul Ticaret University, Istanbul 34445, Turkey

⁷ Section of Mathematics, International Telematic University Uninettuno, Corso Vittorio Emanuele II, 39, Roma 00186, Italy

Corresponding Author Email: chutaratt@nmu.ac.th

<https://doi.org/10.18280/acsm.460107>

ABSTRACT

Received: 12 January 2022

Accepted: 23 February 2022

Keywords:

DMFC, COMSOL, numerical simulation, catalytic layer, diffusion layer

The current work investigates the efficiency of a Direct Methanol Fuel Cell (DMFC) by using COMSOL. The set-up model takes into consideration the electrochemical kinetics and chemical reactions. The anode catalyst layers are a main element in the PEM fuel cell; their porosity significantly affects the fuel cell efficiency. We focus on the impact of catalytic layers porosity on the battery efficiency. As claimed by the results, the porosity of catalytic layer greatly affects the performance of the battery. In addition, better output performance of μ DMFC may be obtained when the catalytic layer porosity is chosen as $\varepsilon_{ACL}=0.009-0.1$. The distributions of methanol, carbon dioxide, water, oxygen, polarization, and the current density are plotted to highlight the impact of porosity on the global performances.

1. INTRODUCTION

Direct Methanol Fuel Cell (DMFC) can greatly reduce battery size, with high energy density and pollution-free, and which is expected to become micro-miniature power supply for small electronics and micro-sensors. However, the practical application of μ DMFC still has to solve many problems, such as low conversion efficiency, low power, methanol permeation, etc. [1]. In addition, the transfer of electrochemical reaction substances into the battery, the influence of the structural parameters of diffusion and catalytic layers of the battery on the efficiency, etc., require extensive research for DMFC to be able to perform at its best [2]. Therefore, numerical analysis and simulation of μ DMFC are particularly important. The University of Newcastle in the UK started studying the theoretical model of μ DMFC earlier. They mainly focused on the one-dimensional model of μ DMFC and first established a one-dimensional model of the gaseous porous electrode μ DMFC [3, 4]. Pennsylvania State University in the United States has proposed a complete two-phase μ DMFC flow model [5]. In recent years, the three-dimensional analysis of DMFC has gradually become the focus of research [6, 7]. The authors discussed the theoretical model of DMFC according to the law of conservation of mass and electrochemistry [8-12]. The COMSOL Multiphysics software allowed performing numerical simulations to study the distribution of substances inside the battery. The modeling of two-phase flows for DMFC is very complicated, as reported

by Murgia et al. [13]. To consider the multiphase flows in the cathodic and anodic layers, it is necessary to introduce the approximate Gaussian function of the capillary pressure [14-16]. Wang and Wang [17] employed a mixing flow model and considered the gas and liquid species to be in thermodynamic equilibrium. Other investigators [18] suggested a model to explore the mass transport in the anode. Divisek et al. [19] employed a model regarding the membrane-electrode of a DMFC cell. Rice and Faghri [20] interested in determining the methanol concentration at the anode. This method has been successful in decreasing the methanol crossover rate. Kazim et al. [21] treated the catalyst layer as a component. Universal government equations applicable to the whole computer field are adopted. The results for the diffusion of methanol and carbon dioxide at the anode, water and oxygen at the cathode and polarization curves and the corresponding current density are presented below [22-25].

COMSOL is being used to examine the efficiency of a Direct Methanol Fuel Cell (DMFC). The electrochemical kinetics and chemical reactions are taken into account in the setup model. The anode catalyst layers are a key component of the PEM fuel cell, and their porosity has a big impact on the efficiency. The impact of catalytic layer porosity on battery efficiency is the focus of this study.

2. PRINCIPLE AND MODEL OF THE BATTERY

Taking μ DMFC as a research object, as given in Figure 1.

The aqueous solution of methanol flows from the anode passes through the anode by diffusion and convection. On the catalytic layer of the anode, methanol is oxidized. Hydrogen ions are carried by water molecules through the proton exchange membrane to reach the cathode and react electrochemically with oxygen to produce water, exhaust gases are evacuated from the canal [26-28].

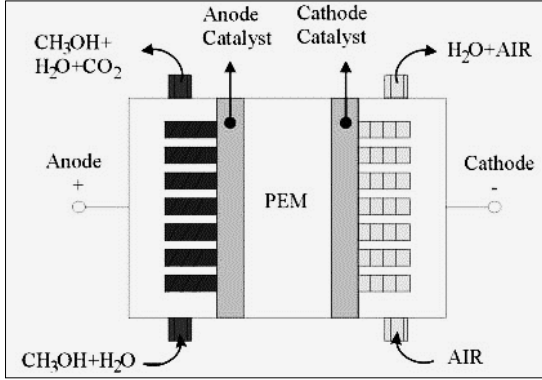
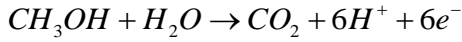


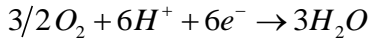
Figure 1. Presentation of DMFC [29]

The generated carbon dioxide returns to the microchannel through the hydrophobic pores of the electrode and is discharged with the aqueous solution. Also, part of the methanol reaches the cathode due to permeation, and reacts directly with oxygen to generate carbon dioxide [30, 31].

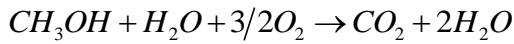
- Anodic oxidation reaction:



- Cathodic reduction reaction:



- The total reaction formula:



3. MATHEMATICAL ISSUES

The domain highlighted in Figure 1 [29], shows the membrane electrode assembly. Note that the channel width and the ribs width are symmetrical about their midpoint. The computational domain is the zone which is bounded by the dotted curves [31-35].

3.1 Main equations

The main equations for modeling the 2D, steady-state, and two-phase phenomenon in the DMFC highlighted in this section [36-39]. The transport of methanol vapor and water vapor was not considered in our model.

Anode porous region:

$$C_{M,l} : \nabla \cdot \left[\begin{pmatrix} -\frac{Kk_{rl}}{\mu_l} \nabla p_l \\ -D_M^{eff} \nabla C_{M,l,a} \end{pmatrix} C_{M,l,a} \right] = \dot{R}_{M,l,a} \quad (1)$$

$$C_{MV,g} : \nabla \cdot \left[\begin{pmatrix} -\frac{Kk_{rg}}{\mu_g} \nabla p_{g,a} \\ -D_{MV,g}^{eff} \nabla C_{MV,g,a} \end{pmatrix} C_{MV,g,a} \right] = \dot{R}_{MV,g,a} \quad (2)$$

$$S_{l,a} : \nabla \cdot \left[\begin{pmatrix} -\frac{Kk_{rg}}{\mu_g / \rho_g} \left(\frac{dp_c}{dS} \nabla S_{l,a} + \nabla p_{l,a} \right) \end{pmatrix} \right]_{\nabla p_{g,a}} = \dot{m}_{g,a} \quad (3)$$

$$p_{l,a} : \nabla \cdot \left[\begin{pmatrix} -\frac{Kk_{rl}}{\mu_l / \rho_l} \nabla p_{l,a} \end{pmatrix} \right] = \dot{m}_{l,a} \quad (4)$$

$$C_{WV,g} : \nabla \cdot \left[\begin{pmatrix} -\frac{Kk_{rg}}{\mu_g} \nabla p_{g,a} \\ -D_{WV,g}^{eff} \nabla C_{WV,g,a} \end{pmatrix} C_{WV,g,a} \right] = \dot{R}_{WV,g,a} \quad (5)$$

Cathode porous region:

$$C_{O_2,g} : \nabla \cdot \left[\begin{pmatrix} -\frac{Kk_{rg}}{\mu_g} \nabla p_{g,c} \\ -D_{O_2,g}^{eff} \nabla C_{O_2,g,c} \end{pmatrix} C_{O_2,g,c} \right] = \dot{R}_{O_2,g,c} \quad (6)$$

$$S_{l,c} : \nabla \cdot \left[\begin{pmatrix} -\frac{Kk_{rl}}{\mu_l / \rho_l} \left(\frac{dp_c}{dS} \nabla S_{l,c} + \nabla p_{g,c} \right) \end{pmatrix} \right]_{\nabla p_{l,c}} = \dot{m}_{l,c} \quad (7)$$

$$p_{g,c} : \nabla \cdot \left[\begin{pmatrix} -\frac{Kk_{rg}}{\mu_g / \rho_g} \nabla p_{g,c} \end{pmatrix} \right] = \dot{m}_{g,c} \quad (8)$$

$$C_{WV,g,c} : \nabla \cdot \left[\begin{pmatrix} -\frac{Kk_{rg}}{\mu_g} \nabla p_{g,c} \\ -D_{WV,g}^{eff} \nabla C_{WV,g,c} \end{pmatrix} C_{WV,g,c} \right] = \dot{R}_{WV,g,c} \quad (9)$$

Membrane:

In the membrane, liquid water should not be neglected as this is generally considered to be a gaseous insulator. The methanol crossover flux is:

$$N_{M,N} \Big|_{MEM/CCL} = \left(\begin{array}{c} -D_{M,N}^{eff} \nabla C_{M,N} \\ +n_{d,w} X_M \frac{I_{proton}}{F} \end{array} \right) \Big|_{MEM/CCL} \quad (10)$$

The flux of water crossover $N_{W,N}$ is given by:

$$N_{W,N} \Big|_{MEM/CCL} = \left(\begin{array}{c} \underbrace{-D_{W,N}^{eff} \cdot \nabla C_{W,N}}_{N_{W,Diffusion}} \\ + n_{d,W} \underbrace{\frac{I_{proton}}{F}}_{N_{W,EOD}} \underbrace{\frac{\rho_W}{M_W} \frac{K}{\mu_W} \frac{\Delta P_{l,CA}}{\delta_{mem}}}_{N_{W,Back-flow}} \end{array} \right) \Big|_{MEM/CCL} \quad (11)$$

Other necessary parameters are detailed in the study of Yang and Zhao [40].

3.2 Boundary details

As shown in Figure 2, we have six limits on the computational domain [40].

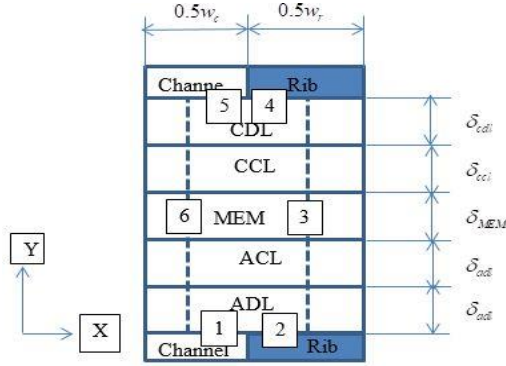


Figure 2. Schematic of model domain calculation [40]

Boundary 1: the entry conditions.

$$\begin{aligned} C_{M,L} &= C_M^{in}, C_{M,V} = C_{M,V}^{in}, C_{W,V} \\ &= C_{W,V}^{in}, P_n = P_l^{in}, s = 1 \end{aligned} \quad (12)$$

Boundary 2: the interface between the anode diffusion layer and the anode rib collector.

$$\begin{aligned} \frac{\partial C_M}{\partial y} &= 0, \frac{\partial C_{M,V}}{\partial y} = 0, \frac{\partial C_{W,V}}{\partial y} = 0, \\ \frac{\partial P_l}{\partial y} &= 0, \frac{\partial s}{\partial y} = 0 \end{aligned} \quad (13)$$

Boundary 4: the cathode rib, where all flows in the direction are zero:

$$\frac{\partial C_{O_2}}{\partial y} = 0, \frac{\partial C_{W,V}}{\partial y} = 0, \frac{\partial P_g}{\partial y} = 0, \frac{\partial s}{\partial y} = 0 \quad (14)$$

Boundary 5: inlet of the oxygen supply and the outlet of the removal of water at the cathode:

$$C_{O_2} = C_{O_2}^{in}, C_{W,V} = C_{W,V}^{in}, P_g = P_g^{in}, s = 0 \quad (15)$$

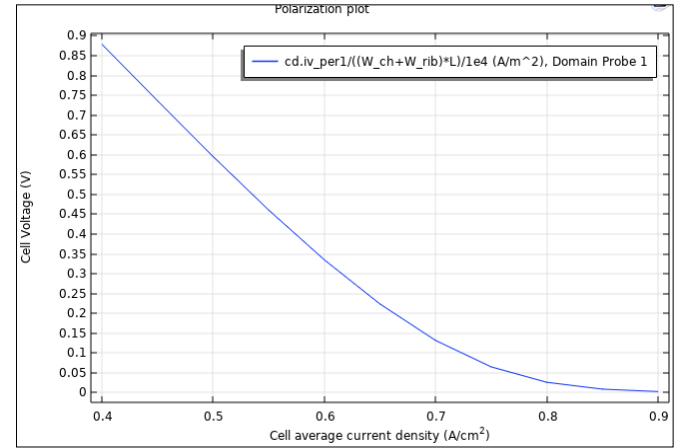
Boundaries 3 and 6: symmetrical condition:

$$\begin{aligned} \frac{\partial C_M}{\partial x} &= 0, \frac{\partial C_{M,V}}{\partial x} = 0, \frac{\partial C_{O_2}}{\partial x} = 0, \\ \frac{\partial C_{W,V}}{\partial x} &= 0, \frac{\partial P_l}{\partial x} = 0, \frac{\partial P_g}{\partial x} = 0, \frac{\partial s}{\partial x} = 0 \end{aligned} \quad (16)$$

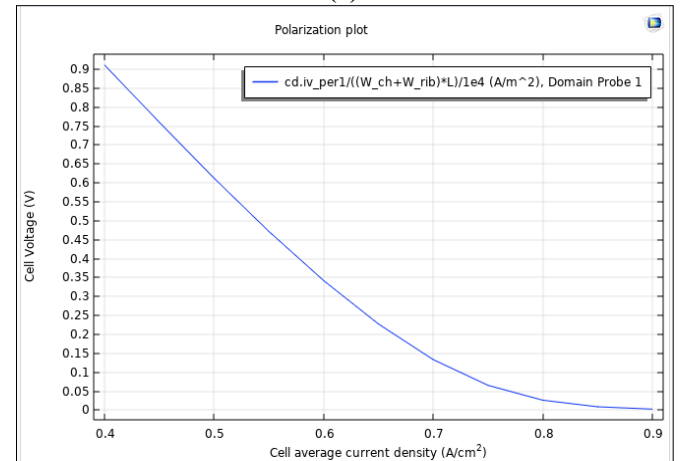
The geometric dimensions of the cell and the operating parameters and the electrochemical properties are also detailed in the study of Yang and Zhao [40]. The governing equations described above are solved numerically using COMSOL - Multiphysics software which has been developed on the basis of the finite element method [41].

4. RESULTS AND DISCUSSION

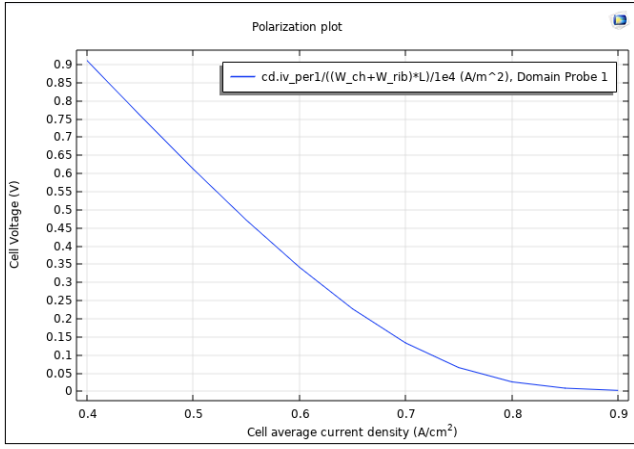
The effects of anodic catalyst layer porosity have been studied numerically in this work. The catalyst layer porosity (CL) can affect the fuel cell efficiency due to the resistance to methanol transport, which is highly depending on it. The highest ACL porosities allow significant quantity of methanol to be transferred with less resistance, reaching thus the reactive zone of ACL and allowing full electrochemical reaction. So, a slight increase for the current density is generated, as shown in Figure 3, where the polarization curves are plotted for different porosities of the CCL anodic catalyst layer ϵ_{ACL} (0.02, 0.04, and 0.1). It can be seen that for a porosity $\epsilon_{ACL} = 0.1$ of the anodic catalyst layer, there will be a high performance for this kind of fuel cells.



(a)

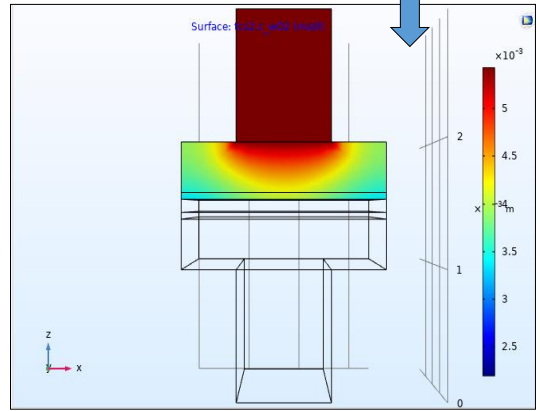
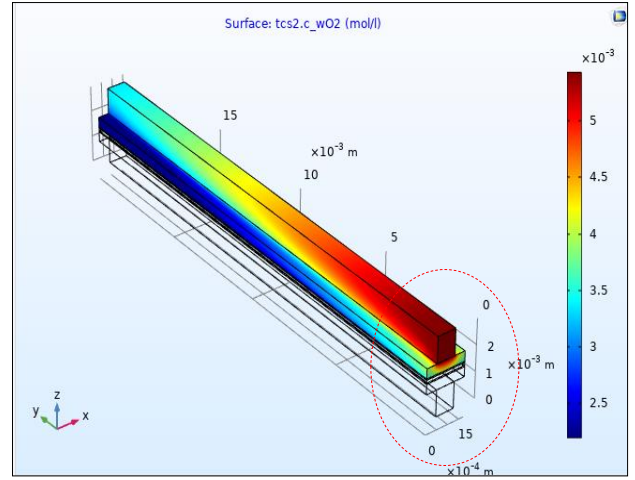


(b)

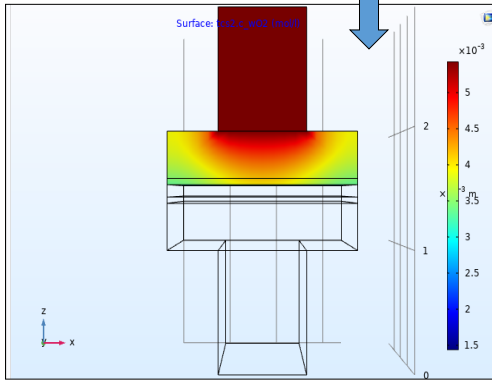
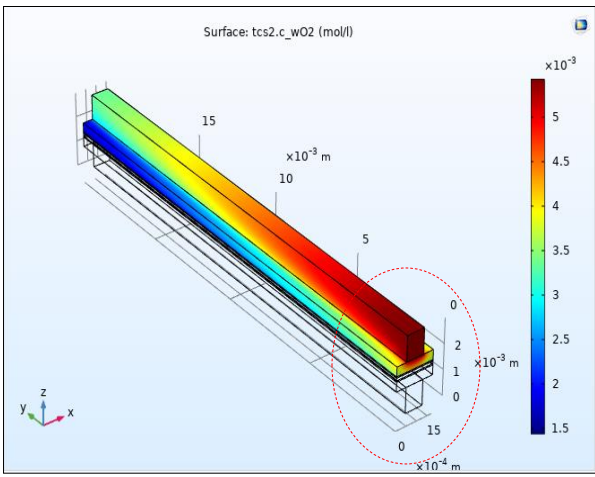


(c)

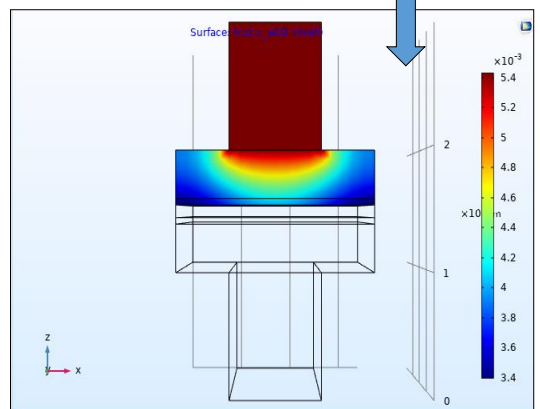
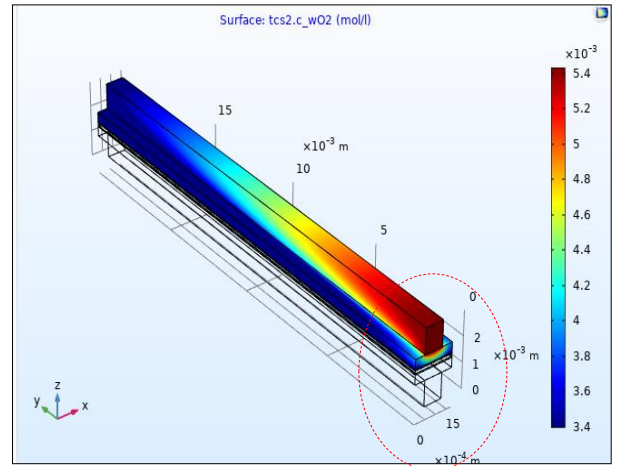
Figure 3. Impact of porosity of the ACL anode catalyst layer on the efficiency of the DMFC fuel cell (a) $\epsilon_{ACL}=0.1$, (b) $\epsilon_{ACL}=0.04$, (c) $\epsilon_{ACL}=0.02$



(b)



(a)

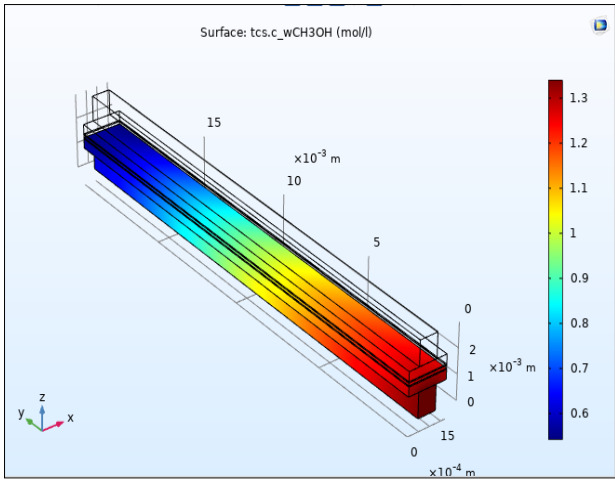


(c)

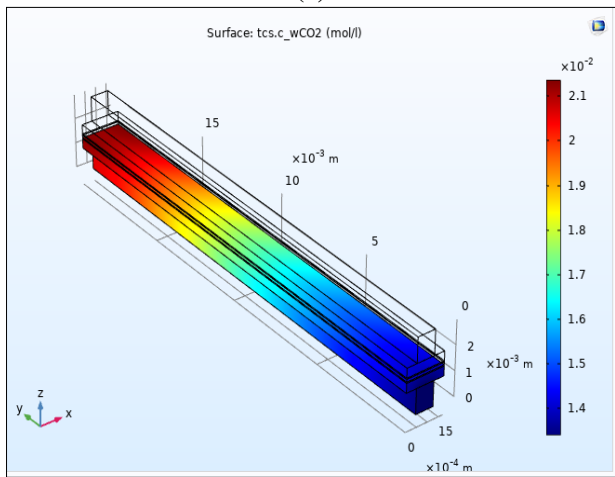
Figure 4. Variation of oxygen concentrations at the cathode with different porosity of anode catalyst layer (a) $\epsilon_{ACL}=0.02$, (b) $\epsilon_{ACL}=0.04$, (c) $\epsilon_{ACL}=0.1$

Figure 4 illustrates the variation of oxygen mole fraction inside the cathode layers. It is clearly demonstrated that as the porosity of the anodic catalyst layer increases, the oxygen mole fraction is reduced from $5(mol/L)$ to $1.5(mol/L)$. Oxygen is quickly consumed with a porosity of $\epsilon_{ACL}=0.1$ resulting in a larger area of the anodic catalyst layer which becomes active with a higher porosity, whereas with a porosity of $\epsilon_{ACL}=0.02$ or $\epsilon_{ACL}=0.04$ a small part of the anode catalyst layer can be actively used. The results of this numerical study are in agreement with the reported experimental values of [36].

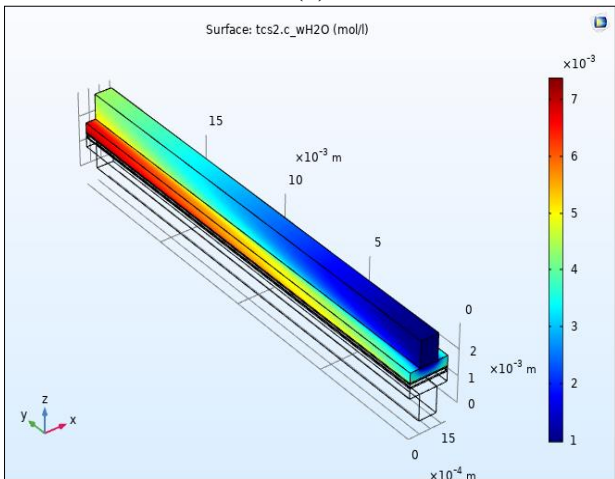
Figure 4. Continued



(a)



(b)

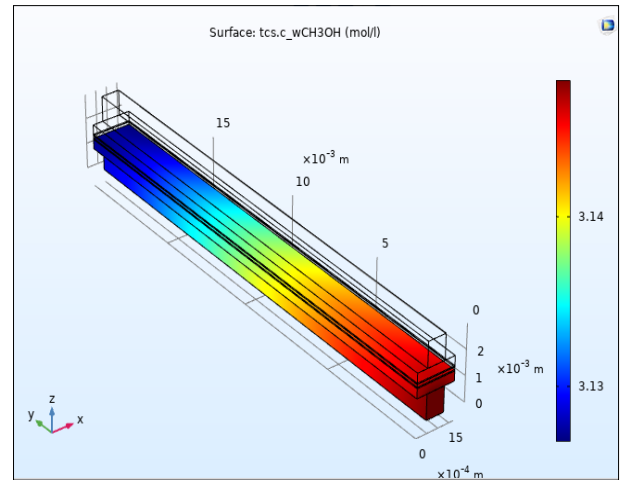


(c)

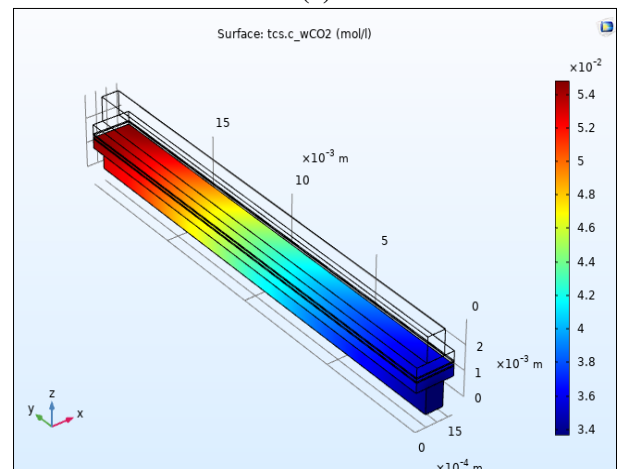
Figure 5. Variation of concentrations of (a) methanol and (b) carbon dioxide, (c) distribution of water with ACL porosities $\epsilon_{ACL}=0.02$ and $\epsilon_{mem}=0.1$

The effects of the porosity of the anode catalyst layer on the distribution of methanol to the anode are also examined. The diffusion curves of the reactants (methanol, water) illustrated in Figures 2-5 for three different porosities of the anodic catalyst layer (ACL) of $\epsilon_{ACL}=(0.1, 0.02, 0.04)$ shows the influence of the latter on the diffusivity of reagents in anodic diffusion layers. The fuel cell with significant ACL porosity widens the diffusion limitation of the reactants (methanol) in the anodic diffusion zones (ADL) while the consumption also increases. And therefore, the consumption of reagents such as

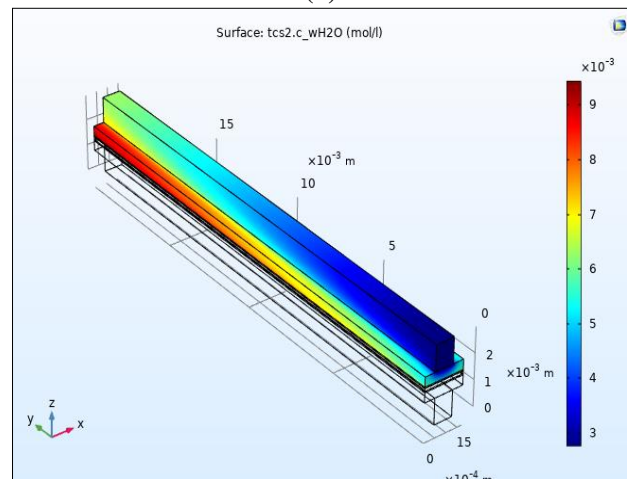
oxygen in the cathode side (cathodic diffusion layer CDL and cathodic catalyst layer CCL) also increases. Note that the increase in methanol must be eliminated or limited for that of the porosity membrane layer which must be in a very limited interval between 0.1 and 0.15 [41].



(a)



(b)



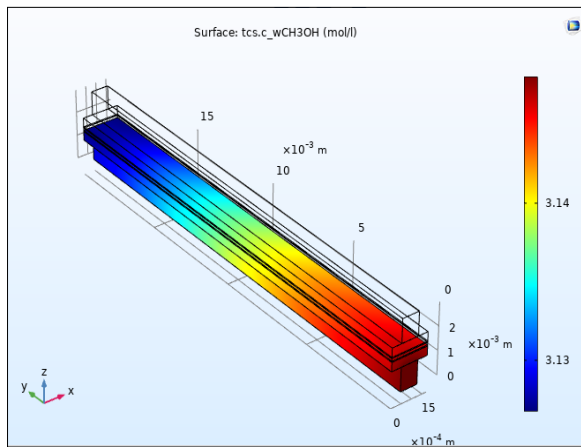
(c)

Figure 6. Variation of concentrations of (a) methanol and (b) carbon dioxide, (c) distribution of water with ACL porosities $\epsilon_{ACL}=0.04$ and $\epsilon_{mem}=0.1$

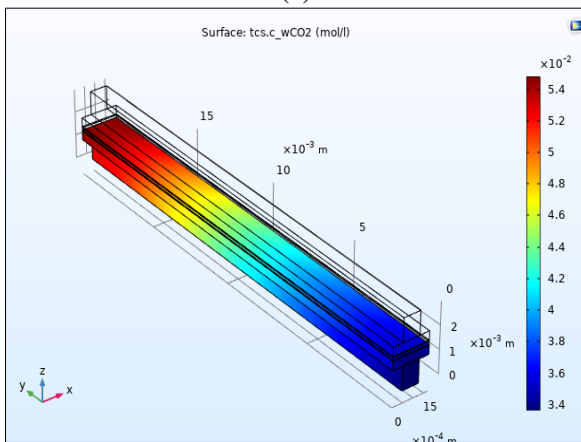
Figures 5-7 reveal the variation of the mole fraction of water at the side of the cathode, and the methanol and carbon dioxide CO_2 at the side of the anode in different porosities of the ACL anodic catalyst layer. The methanol mole fraction augments

with the significant porosity of the anode catalyzer layer $\epsilon_{CCL}=0.1$ than in the case of a porosity of $\epsilon_{CCL}=0.4$, and $\epsilon_{CCL}=0.02$. The same behavior is observed for oxygen and other products resulting from electrochemical reactions.

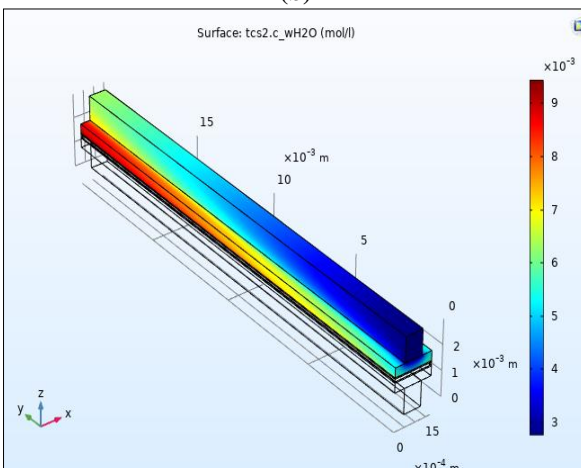
Figure 5 shows again that for a larger ACL porosity we will have an upper limiting current density a $9A/cm^2$, because a lower current density is produced with a lower porosity due to the reduced diffusion of methanol in the catalyst. The considerable volume porosity positively affects the oxygen mass transport in the cathode side as well as methanol in the anode side. This methanol permutation yields a growth in methanol, resulting in a parasitic current and decreased performance of the DMFC battery.



(a)



(b)



(c)

Figure 7. Variation of concentrations of (a) methanol and (b) carbon dioxide, (c) distribution of water with ACL porosities $\epsilon_{ACL}=0.1$ and $\epsilon_{mem}=0.1$

For carbon dioxide CO_2 , note that the latter affects considerably the methanol displacement towards the cathodic side of which the growth of methanol results, because it plays the role of a barrier to the diffusion of methanol. So, the increase in CO_2 is significant in some way.

The cell power density vs. different porosities ($\epsilon_{ACL}=0.02$, 0.04 , and 0.1) is given in Figure 6. The increased porosity yields an increase in power density, and consequently, significant peak power densities are obtained. To maintain the highest efficiency, the fuel cell operates at $0.04 \leq \epsilon_{ACL} \leq 0.1$. Interestingly, the experimental data reveal a continuous augmentation in power with increased current density [42].

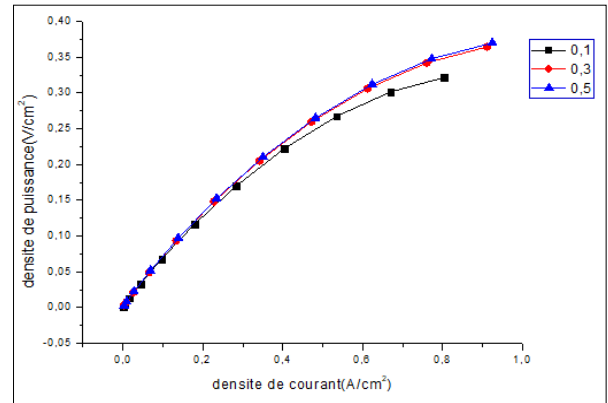


Figure 8. Fuel cell performance, power density (V/cm^2) as a function of current density (A/cm^2)

Our conclusion in this case is to use the average porosity to avoid having the phenomenon of increased methanol on the one hand and to have the highest yield for this battery on the other hand. So, we will take the porosity $\epsilon_{ACL} = 0.07$, in Figure 8.

5. CONCLUSION

This paper used the COMSOL Multiphysics software to explore the performance of DMFC for the direct methanol micro fuel cell, and to determine the distribution of the reactants on both sides of the cathode and the anode. On this basis, the impact of the structural parameters of the catalytic layer on the efficiency and the outputs of the battery are analyzed.

Compared to the structure of the catalytic layer, the parameters of this structure have a more complex influence on the performance and output of the battery during the process of transferring reagents and products inside the battery. From the simulation analysis, it can be seen that for DMFC, the porosity of the catalytic layer should be between $\epsilon_{ACL} = 0.04$ and 0.1 .

The catalytic layer is not as complicated as the diffusion layer in the mass transfer process, but it is also very important to determine the porosity of the catalytic layer. A catalytic layer with very high porosity will not help improve the performance of the battery and will enhance the amount of water and flooding of the membrane.

The simulation analysis of the diffusion layer and the catalytic layer provides theoretical guidance for the study of the use of alumina and other materials to perform experiments with porous composite membranes [30] and charged Pt. of carbon, in particular when determining the porosity of the catalytic layer and the amount of Pt.

ACKNOWLEDGEMENT

Chutarat Tearnbucha would like to acknowledge financial support by Navamindradhiraj University through the Navamindradhiraj University Research Fund (NURF).

REFERENCES

- [1] Hosseinpour, M., Sahoo, M., Perez-Page, M., Baylis, S.R., Patel, F., Holmes, S.M. (2019). Improving the performance of direct methanol fuel cells by implementing multilayer membranes blended with cellulose nanocrystals. *International Journal of Hydrogen Energy*, 44(57): 30409-30419. <https://doi.org/10.1016/j.ijhydene.2019.09.194>
- [2] Goor, M., Menkin, S., Peled, E. (2019). High power direct methanol fuel cell for mobility and portable applications. *International Journal of Hydrogen Energy*, 44(5): 3138-3143. <https://doi.org/10.1016/j.ijhydene.2018.12.019>
- [3] Perez-Page, M., Sahoo, M., Holmes, S.M. (2019). Single layer 2D crystals for electrochemical applications of ion exchange membranes and hydrogen evolution catalysts. *Advanced Materials Interfaces*, 6(7): 1801838. <https://doi.org/10.1002/admi.201801838>
- [4] Prapainainar, P., Pattanapisutkun, N., Prapainainar, C., Kongkachuichay, P. (2019). Incorporating graphene oxide to improve the performance of Nafion-mordenite composite membranes for a direct methanol fuel cell. *International Journal of Hydrogen Energy*, 44(1): 362-378. <https://doi.org/10.1016/j.ijhydene.2018.08.008>
- [5] Xu, X., Zhao, G., Wang, H., Li, X., Feng, X., Cheng, B., Yin, Y. (2019). Bio-inspired amino-acid-functionalized cellulose whiskers incorporated into sulfonated polysulfone for proton exchange membrane. *Journal of Power Sources*, 409: 123-131. <https://doi.org/10.1016/j.jpowsour.2018.11.003>
- [6] Sharifi, S., Rahimi, R., Mohebbi-Kalhor, D., Colpan, C.O. (2018). Numerical investigation of methanol crossover through the membrane in a direct methanol fuel cell. *Iranian Journal of Hydrogen & Fuel Cell*, 5(1): 21-33. <https://doi.org/10.22104/IJHFC.2018.2867.1170>
- [7] Prapainainar, P., Maliwan, S., Sarakham, K., Du, Z., Prapainainar, C., Holmes, S.M., Kongkachuichay, P. (2018). Homogeneous polymer/filler composite membrane by spraying method for enhanced direct methanol fuel cell performance. *International Journal of Hydrogen Energy*, 43(31): 14675-14690. <https://doi.org/10.1016/j.ijhydene.2018.05.173>
- [8] Weber, A.Z., Newman, J. (2006). Coupled thermal and water management in polymer electrolyte fuel cells. *Journal of The Electrochemical Society*, 153(12): A2205. <https://doi.org/10.1149/1.2352039>
- [9] Hickner, M.A., Siegel, N.P., Chen, K.S., Hussey, D.S., Jacobson, D.L., Arif, M. (2008). Understanding liquid water distribution and removal phenomena in an operating PEMFC via neutron radiography. *Journal of The Electrochemical Society*, 155(3): B294. <https://doi.org/10.1149/1.2825298>
- [10] Zaffou, R., Jung, S.Y., Kunz, H.R., Fenton, J.M. (2006). Temperature-driven water transport through membrane electrode assembly of proton exchange membrane fuel cells. *Electrochemical and Solid-State Letters*, 9(9): A418. <https://doi.org/10.1149/1.2218306>
- [11] Thomas, A. (2012). Transferts d'eau et de chaleur dans une pile à combustible à membrane: mise en évidence expérimentale du couplage et analyse des mécanismes (Doctoral dissertation, Université de Lorraine). <https://tel.archives-ouvertes.fr/tel-00820468>
- [12] Kandlikar, S.G., Lu, Z., Rao, N., Sergi, J., Rath, C., McDade, C., Herescu, A. (2010). Visualization of fuel cell water transport and performance characterization under freezing conditions (No. DOE/GO/17018). Rochester Inst. of Technology, Rochester, NY (United States).
- [13] Murgia, G., Pisani, L., Shukla, A.K., Scott, K. (2003). A numerical model of a liquid-feed solid polymer electrolyte DMFC and its experimental validation. *Journal of the Electrochemical Society*, 150(9): A1231. <https://doi.org/10.1149/1.1596951>
- [14] Wang, Y., Wang, C.Y. (2006). A nonisothermal, two-phase model for polymer electrolyte fuel cells. *Journal of the Electrochemical Society*, 153(6): A1193. <https://doi.org/10.1149/1.2193403>
- [15] Wang, C.Y., Cheng, P. (1997). Multiphase flow and heat transfer in porous media. In *Advances in Heat Transfer*, 30: 93-196. [https://doi.org/10.1016/S0065-2717\(08\)70251-X](https://doi.org/10.1016/S0065-2717(08)70251-X)
- [16] Liu, F., Lu, G., Wang, C.Y. (2006). Low crossover of methanol and water through thin membranes in direct methanol fuel cells. *Journal of the Electrochemical Society*, 153(3): A543. <https://doi.org/10.1149/1.2161636>
- [17] Wang, Z.H., Wang, C.Y. (2003). Mathematical modeling of liquid-feed direct methanol fuel cells. *Journal of the Electrochemical Society*, 150(4): A508. <https://doi.org/10.1149/1.1559061>
- [18] Birgersson, E., Nordlund, J., Vynnycky, M., Picard, C., Lindbergh, G. (2004). Reduced two-phase model for analysis of the anode of a DMFC. *Journal of the Electrochemical Society*, 151(12): A2157. <https://doi.org/10.1149/1.1819834>
- [19] Divisek, J., Fuhrmann, J., Gärtner, K., Jung, R. (2003). Performance modeling of a direct methanol fuel cell. *Journal of the Electrochemical Society*, 150(6): A811. <https://doi.org/10.1149/1.1572150>
- [20] Rice, J., Faghri, A. (2006). A transient, multi-phase and multi-component model of a new passive DMFC. *International Journal of Heat and Mass Transfer*, 49(25-26): 4804-4820. <https://doi.org/10.1016/j.ijheatmasstransfer.2006.06.003>
- [21] Kazim, A., Liu, H.T., Forges, P. (1999). Modelling of performance of PEM fuel cells with conventional and interdigitated flow fields. *Journal of Applied Electrochemistry*, 29(12): 1409-1416. <https://doi.org/10.1023/A:1003867012551>
- [22] Yang, W.W., Zhao, T.S., Xu, C. (2007). Three-dimensional two-phase mass transport model for direct methanol fuel cells. *Electrochimica Acta*, 53(2): 853-862. <https://doi.org/10.1016/j.electacta.2007.07.070>
- [23] Burstein, G.T., Barnett, C.J., Kucernak, A.R., Williams, K.R. (1997). Aspects of the anodic oxidation of methanol. *Catalysis Today*, 38(4): 425-437. [https://doi.org/10.1016/S0920-5861\(97\)00107-7](https://doi.org/10.1016/S0920-5861(97)00107-7)
- [24] Wasmus, S., Küver, A. (1999). Methanol oxidation and direct methanol fuel cells: A selective review. *Journal of Electroanalytical Chemistry*, 461(1-2): 14-31.

- [https://doi.org/10.1016/S0022-0728\(98\)00197-1](https://doi.org/10.1016/S0022-0728(98)00197-1)
- [25] Liu, L., Pu, C., Viswanathan, R., Fan, Q., Liu, R., Smotkin, E.S. (1998). Carbon supported and unsupported Pt–Ru anodes for liquid feed direct methanol fuel cells. *Electrochimica Acta*, 43(24): 3657-3663. [https://doi.org/10.1016/S0013-4686\(98\)00123-6](https://doi.org/10.1016/S0013-4686(98)00123-6)
- [26] Arico, A.S., Creti, P., Modica, E., Monforte, G., Baglio, V., Antonucci, V. (2000). Investigation of direct methanol fuel cells based on unsupported Pt–Ru anode catalysts with different chemical properties. *Electrochimica Acta*, 45(25-26): 4319-4328. [https://doi.org/10.1016/S0013-4686\(00\)00531-4](https://doi.org/10.1016/S0013-4686(00)00531-4)
- [27] Chu, D., Jiang, R. (2002). Novel electrocatalysts for direct methanol fuel cells. *Solid State Ionics*, 148(3-4): 591-599. [https://doi.org/10.1016/S0167-2738\(02\)00124-8](https://doi.org/10.1016/S0167-2738(02)00124-8)
- [28] Narayanan, S.R., Frank, H., Jeffries-Nakamura, B., Smart, M., Chun, W., Halpert, G., Kosek, J., Cropley, C., in: *Proton Conducting Membrane Fuel Cells I*, edited by Gottesfeld, S., Halpert, G., Landgrebe, A.R. (PV 95-23, 278, The Electrochem. Soc. Proc. Series, Pennington, NJ 1995).
- [29] Ordonez, M., Iqbal, M.T., Quaicoe, J.E., Lye, L.M. (2006). Modeling and optimization of direct methanol fuel cells using statistical design of experiment methodology. In *2006 Canadian Conference on Electrical and Computer Engineering*, pp. 1120-1124. <https://doi.org/10.1109/CCECE.2006.277802>
- [30] Wang, J.T., Wasmus, S., Savinell, R.F. (1996). Real-time mass spectrometric study of the methanol crossover in a direct methanol fuel cell. *Journal of the Electrochemical Society*, 143(4): 1233. <https://doi.org/10.1149/1.1836622>
- [31] Hikita, S., Yamane, K., Nakajima, Y. (2001). Measurement of methanol crossover in direct methanol fuel cell. *Jsae Review*, 22(2): 151-156. [https://doi.org/10.1016/S0389-4304\(01\)00086-8](https://doi.org/10.1016/S0389-4304(01)00086-8)
- [32] Lu, G.Q., Wang, C.Y., Yen, T.J., Zhang, X. (2004). Development and characterization of a silicon-based micro direct methanol fuel cell. *Electrochimica Acta*, 49(5): 821-828. <https://doi.org/10.1016/j.electacta.2003.09.036>
- [33] Argyropoulos, P., Scott, K., Taama, W.M. (1999). Gas evolution and power performance in direct methanol fuel cells. *Journal of Applied Electrochemistry*, 29(6): 663-671. <https://doi.org/10.1023/A:1003589319211>
- [34] Lu, G.Q., Wang, C.Y. (2004). Electrochemical and flow characterization of a direct methanol fuel cell. *Journal of Power Sources*, 134(1): 33-40. <https://doi.org/10.1016/j.jpowsour.2004.01.055>
- [35] Kulikovskiy, A.A., Divisek, J., Kornyshev, A.A. (2000). Two-dimensional simulation of direct methanol fuel cell. A new (embedded) type of current collector. *Journal of the Electrochemical Society*, 147(3): 953. <https://doi.org/10.1149/1.1393297>
- [36] Kulikovskiy, A.A. (2000). Two-dimensional numerical modelling of a direct methanol fuel cell. *Journal of Applied Electrochemistry*, 30(9): 1005-1014. <https://doi.org/10.1023/A:1004086402501>
- [37] Wang, Z.H., Wang, C.Y., Chen, K.S. (2001). Two-phase flow and transport in the air cathode of proton exchange membrane fuel cells. *Journal of Power Sources*, 94(1): 40-50. [https://doi.org/10.1016/S0378-7753\(00\)00662-5](https://doi.org/10.1016/S0378-7753(00)00662-5)
- [38] Liu, W., Wang, C.Y. (2007). Three-dimensional simulations of liquid feed direct methanol fuel cells. *Journal of the Electrochemical Society*, 154(3): B352. <https://doi.org/10.1149/1.2429041>
- [39] Yuan, J., Sundén, B. (2005). Analysis of intermediate temperature solid oxide fuel cell transport processes and performance. *Journal of Heat Transfer*, 127: 1380-1390. <https://doi.org/10.1115/1.2098847>
- [40] Yang, W.W., Zhao, T.S. (2008). A transient two-phase mass transport model for liquid feed direct methanol fuel cells. *Journal of Power Sources*, 185(2): 1131-1140. <https://doi.org/10.1016/j.jpowsour.2008.07.052>
- [41] Wang, Z.H., Wang, C.Y. (2003). Mathematical modeling of liquid-feed direct methanol fuel cells. *Journal of the Electrochemical Society*, 150(4): A508. <https://doi.org/10.1149/1.1559061>
- [42] Kharton, V.V., Marques, F.M.B., Atkinson, A. (2004). Transport properties of solid oxide electrolyte ceramics: a brief review. *Solid State Ionics*, 174(1-4): 135-149. <https://doi.org/10.1016/j.ssi.2004.06.015>